Chapter

Self-Assembly of GeMn Nanocolumns in GeMn Thin Films

Thi Giang Le

Abstract

This chapter presents the results of growing GeMn nanocolumns on Ge(001) substrates by means of molecular beam epitaxy (MBE). The samples have been prepared by co-depositing Ge and Mn at growth temperature of 130°C and Mn at concentration of ~6% to ensure the reproduction of GeMn nanocolumns. Based on the observation of changes in reflection high-energy electron diffraction (RHEED) patterns during nanocolumn growth, surface signals of GeMn nanocolumn formation have been identified. Structural analysis using transmission electron microscopy (TEM) show the self-assembled nanocolumns with core-shell structure extend through the whole thickness of the GeMn layer. Most of nanocolumns are oriented perpendicular to the interface along the growth direction. The nanocolumn size has been determined to be about 5–8 nm in diameter and a maximum height of 80 nm. A phenomenological model has been proposed to explain the driving force for self-assembly and growth mechanisms of GeMn nanocolumns. The in-plane or lateral Mn diffusion/segregation is driven by a low solubility of Mn in Ge while the driving force of Mn vertical segregation is induced by the surfactant effect along the [001] direction.

Keywords: GeMn nanocolumns, Ge thin film, growth mechanism, Mn segregation, Mn low solubility, Mn_5Ge_3 clusters

1. Introduction

The discovery of the giant magneto-resistance (GMR) effect in metallic multilayers by Albert Fert and Peter Grunberg has probably made a great step toward spintronics [1, 2]. To further extend applications of spintronics, researchers and engineers invent new architectures and structures, allowing to realize the integration of magnetic materials into semiconductors. The development of active spin devices, such as spin transistors or diodes, calls for new materials, which enable to efficiently inject spin-polarized currents into standard semiconductors. Two main ways have been explored in order to inject spin-polarized current into semiconductors.

Firstly, one can make use of the properties of a ferromagnetic metal (FM) such as Co, Fe, Ni, or their alloys. Spin-polarized currents tunnel from ferromagnetic metal to semiconductor through an insulator [3, 4] or a Schottky barrier [5]. However, the efficiency of spin injection directly into Si or Ge remains very low. Indeed, most of the ferromagnetic metals react with Si and Ge, leading to the formation of interfacial silicides or germanides, which, for most of them, are not ferromagnetic. It is also not trivial to obtain epitaxial growth of an oxide in

between Ge (or Si) and a ferromagnetic metal; spin injection is therefore limited by the interface roughness [6].

Secondly, diluted magnetic semiconductors (DMSs), obtained by doping standard semiconductors with magnetic impurities, such as Mn or Co, have emerged as potential candidates for spin injection. The materials become ferromagnetic while conserving their semiconducting properties. They exhibit therefore natural impedance match to host semiconductors and are expected to efficiently inject spin-polarized currents into semiconductors. Since the spintronic devices often operate at room temperature and they are heated up during the operation, the great challenge and ultimate goal of the research in this field is to obtain DMSs exhibiting ferromagnetism well above room temperature. This feature represents key issues for the development of spintronic devices.

In the 1990s, DMSs of III-V-based compound semiconductors were successfully fabricated by introducing Mn ions, but Mn atoms are much less soluble than in II-VI semiconductors, making them difficult to be diluted in the III-V semiconductor, such as (GaMn)As. By using a low-temperature MBE technique, it is possible to grow thin films with higher Mn concentrations in a nonequilibrium process and prevent Mn ions to form precipitations. The T_C, achieved at that time, was 110 K for 5.5% Mn-doped GaAs [7]. So far, the GaMnAs diluted magnetic semiconductors seem to be the most important and the best understood system up to now. However, they are ferromagnetic only at temperatures well below room temperature, the highest value reported was 173 K by Gallagher's group in UK [8]. An interesting alternative could be magnetic semiconductors that are based on elemental semiconductors and also owe to their compatibility with Si microelectronics. In the last decades, considerable amount of work has been devoted to the synthesis of Mn-doped Ge and Si, such as SiMn, GeMn, and SiGeMn. The main motivations for the synthesis of these materials are:

- Compatibility with mainstream silicon technology.
- Mn magnetic impurity acts as an acceptor in the substitutional sites in the crystal lattice.
- Very long spin relaxation time, which comes from weak spin-orbital coupling in Si and Ge [9]. It is worth noting that the spin relaxation time in IV-IV semiconductors is much larger than that in III-V semiconductors.

Although silicon is the key material of microelectronics, the first demonstration of spin injection was only achieved in 2007. Until now, it is unclear whether Mn can substitute Si sites since Mn ions in Si are fast interstitial diffusers even at low temperatures. Experimentally, numerous groups have reported the observation of ferromagnetism in Mn-doped Si with Curie temperatures ranging from 200 to 400 K [10–13]. However, the origin of the observed ferromagnetism remains very diverse, which makes Mn-doped Si DMSs difficult to be realized.

Recently, special attention both in experiment and theory has been given to group-IV $Ge_{1-x}Mn_x$ diluted magnetic semiconductors due to their compatibility with mainstream Si-based electronics. Zwicker et al. conducted the first study on the Ge-Mn equilibrium phase in the early 1949 [14]. Later on followed extensive investigations establishing the relative phase diagram [15]. The interests in GeMn system as a promising high-T_C ferromagnetic semiconductor essentially started in 2002 with the publication by Park et al. [16], claiming the fabrication of a GeMn DMS with a T_C up to 116 K and linear dependence on the Mn concentration. Since

then, many publications investigated different aspects of the GeMn system and employed different fabrication techniques [17–19].

Despite numerous researches carried out up to now, the fabrication of homogeneous and high-T_C $Ge_{1-x}Mn_x$ films remains a challenge. It is now commonly believed that secondary phases form once the Mn concentration exceeds the solubility limit [20]. In general, when the Mn concentration and the growth temperature are high enough or after post-annealing, parasitical metallic nanoclusters of Mn_5Ge_3 are observed in GeMn films [21–23]. $Mn_{11}Ge_8$ precipitates are observed under certain conditions [24]. A result of particular interest is the discovery of the CEA group on the formation of a nanocolumn phase, which exhibits a Curie temperature higher than 400 K [25]. The nanocolumns have an average size of 5 nm and are separated from each other by a distance of about 8 nm. This phase has been attributed to a new compound, Ge_2Mn, which does not exist in the Ge-Mn phase diagram.

Among numerous phases of GeMn DMS, the nanocolumns' phase appears to be the most interesting, because it is the unique phase that has Tc higher than RT. But concerning the GeMn nanocolumns, there are some remaining questions about the composition and the mechanism of nanocolumn formation. One of the main objectives of this chapter consists of understanding the origin of the formation of this nanocolumn phase. Our purposes are to determine the nanocolumn size, driving force for self-assembly, and growth mechanisms of GeMn nanocolumns.

2. Literature review of the synthesis of $Ge_{1-x}Mn_x$ DMS

After the first report of ferromagnetism in the $Ge_{1-x}Mn_x$ system with T_C = ~116 K [16], the synthesis of $Ge_{1-x}Mn_x$ DMSs has been the subject of numerous investigations [26–36]. Since it has been shown in Ref. 10 that magnetic ordering in $Ge_{1-x}Mn_x$ linearly increases with increasing Mn concentration, a number of works have focused on investigations of the dependence of the Curie temperature of GeMn DMS on the growth parameters. Among numerous growth parameters, which can affect the $Ge_{1-x}Mn_x$ growth behavior, the growth temperature and the Mn concentration appear to be the most important. Before presenting our results, we summarize below some major results, reporting on the influence of these two parameters on the growth and magnetic properties of GeMn DMSs.

2.1 Effects of Mn concentration on the growth behavior of $Ge_{1-x}Mn_x$ DMS

Similar to the case of Mn in III-V semiconductors, the solid solubility of Mn in Ge is as low as 10^{15} cm^{-3} under equilibrium conditions [37]. As a consequence of such a low solubility, thin film growers use low-temperature growth to bring the system to high nonequilibrium conditions with the hope to increase the Mn concentration that can be incorporated in the films. Low-temperature growth is also expected to minimize phase separation and/or the formation of unwanted compounds. However, it is worth noting that low-temperature growth often conducts to the formation of metastable state and low crystalline quality of epilayers due to a low surface diffusion coefficient of adatoms on surface. Moreover, the ratio between interstitial and substitutional dopants may be reduced due to a too low growth temperature.

Several reports have shown that a concentration of holes up to 10^{17}–10^{20} cm^{-3} can be obtained when doping Mn in Ge [16, 25, 29, 30, 38, 39]. It has also been demonstrated that when Mn atoms substitute Ge sites, Mn ions are in 2+ ionic states [35, 36, 40, 41]. Li et al. [38] reported on Mn ionic implantation in Ge and

suggested that up to 20–30% Mn ions could be incorporated in substitutional sites and post-annealing allowed increasing this fraction to 40–50%. Some interstitial Mn ions can be converted to substitutional Mn under adequate post-annealing.

In general, it is now generally accepted by the scientific community working on GeMn DMSs that a Mn concentration up to 5–9% can be incorporated in Ge layers without creating visible metallic clusters or precipitates, such as Mn_5Ge_3 and $Mn_{11}Ge_8$. However, other kinds of Mn-rich cluster phases, in particular with size being in the range of sub-nanometer, may exist [41–43]. A question, which is still under debate, concerns the exact Mn amount or concentration that really participates in producing ferromagnetic ordering in $Ge_{1-x}Mn_x$ materials. Answering this question certainly requires nano-scaled characterization tools for both structural and magnetic properties. Another remaining question concerns the origin of ferromagnetism in $Ge_{1-x}Mn_x$. If the Zener model or hole-mediated ferromagnetic model, which uses thermodynamic and micro-magnetic descriptions to explain the origin of ferromagnetism in DMS materials, is generally accepted, other mechanisms, for example bound magnetic polarons, have been proposed [36]. These authors, by combining magnetic and transport characterizations of $Ge_{1-x}Mn_x$ films doped with ~5% of Mn, provided the existence of two magnetic transitions: T_C^* (~112 K) and T_C (~12 K) of the layers. The transition at high temperature (T_C^*) can be attributed to the exchange interaction between localized charge carriers and surrounding Mn ions (magnetic polarons) while the T_C transition may arise from infinite-size ferromagnetic clusters due to inhomogeneous distribution of Mn dopants inside the layers.

2.2 Effects of growth temperature on $Ge_{1-x}Mn_x$ DMS

Together with the Mn concentration, the growth temperature is recognized as one of the main parameters that governs the growth process of GeMn films. In particular, the growth temperature has a direct consequence on the nature of phase separation or clusters that are formed in the layers: nano-scaled Mn-rich regions or metallic clusters (Mn_5Ge_3, $Mn_{11}Ge_8$ or Mn_5Ge_2). According to previous works, three main regions of the growth temperature can be classified: (i) above 180°C, (ii) below 80°C, and (iii) intermediate temperatures in the range from 110 to 150°C.

The most "famous" or the most frequently observed Mn-Ge clusters are certainly metallic Mn_5Ge_3 clusters. This phase of clusters is generally observed when the growth temperature exceeds 180°C. **Figure 1** shows an example in which a high density of Mn_5Ge_3 clusters is present in $Ge_{1-x}Mn_x$ films, which were grown at 225°C and contained a Mn concentration of 3% [23]. Using transmission electron diffraction (TED) and magnetic characterizations, the authors have unambiguously identified that those clusters are made of the Mn_5Ge_3 phase. An epitaxial relationship between these clusters and Ge(001) has been determined: a majority of them are oriented with the hexagonal (0001) plane of Mn_5Ge_3 being aligned with the (001) plane of Ge while some others are randomly distributed in the layers (see **Figure 1**) (right).

In the low growth temperature range, Bougeard et al. [42] reported that $Ge_{1-x}Mn_x$ films were free of intermetallic precipitates but a new kind of cluster was formed. **Figure 2a** shows a plan-view TEM image of a $Ge_{1-x}Mn_x$ film grown at 60°C with Mn content of 5%. Numerous areas exhibiting slightly darker contrast are observed; these areas were found to be coherently bounded to the surrounding Ge matrix. Analyses performed with annular dark field by scanning transmission electron microscopy (STEM) on a single cluster string (**Figure 2b**) revealed high structural disorder around the clusters, suggesting that they have a strained shell

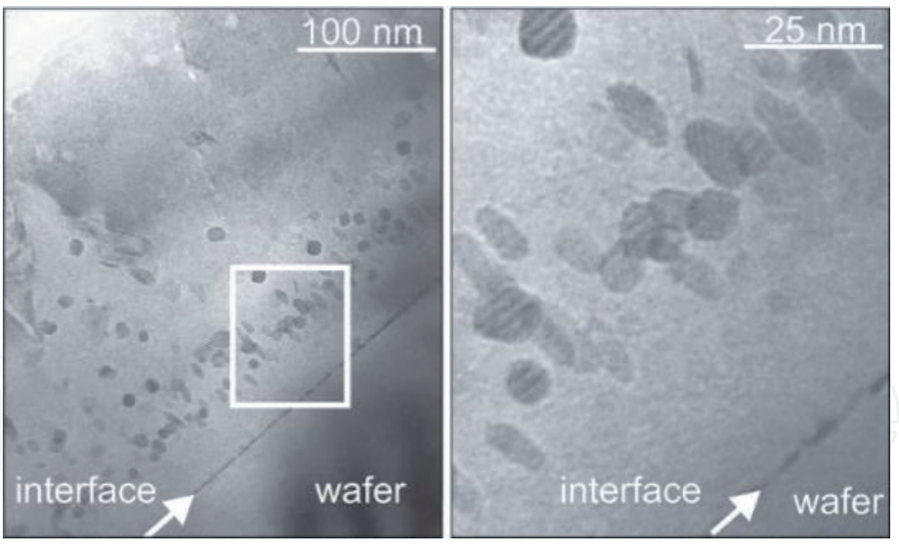

Figure 1.
TEM images of a $Ge_{0.97}Mn_{0.03}$ epilayer on a Ge wafer (left) with a magnified section (right). The arrows mark the interface between the wafer and epilayer [27].

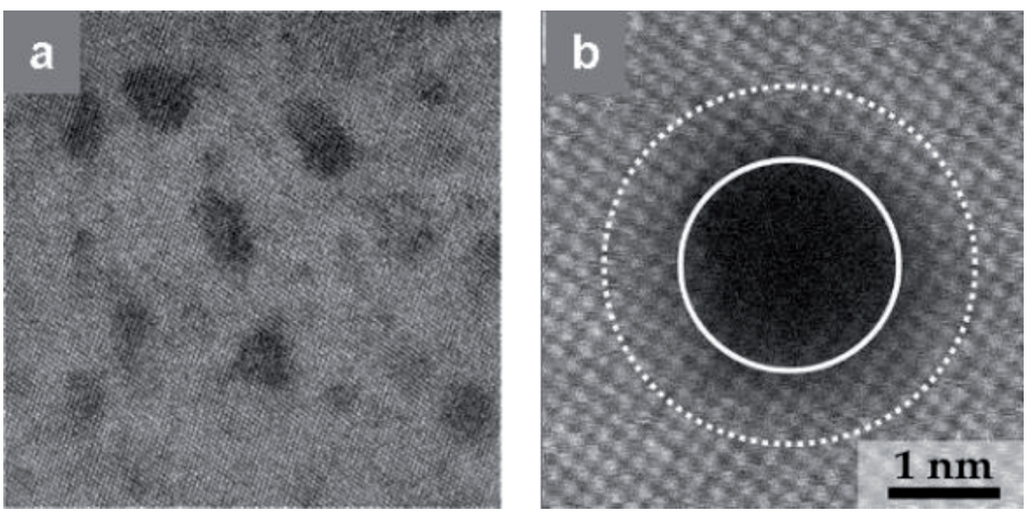

Figure 2.
High-resolution plan-view STEM images of $Ge_{0.927}Mn_{0.073}$ sample grown at 60°C. Mn-rich regions with darker contrast are amorphous Mn [44].

with a core made up by amorphous Mn [32]. Continuing their investigations, the authors recently showed that when the growth temperature increased to 85–120°C, metallic Mn_5Ge_3 in the shape of nanometer-sized inclusions can be formed in a diluted $Ge_{1-x}Mn_x$ matrix [45]. It is worth noting that when post-annealing was carried out on $Ge_{1-x}Mn_x$ films grown at the temperature range of 70–120°C, new kinds of clusters, $Mn_{11}Ge_8$ and Mn_5Ge_2 can be formed near the surface region.

A result of particular interest, observed in the intermediate temperature range from 110 to 150°C, is the observation by Jamet and colleagues at CEA-Grenoble of highly elongated precipitates, which are self-organized to form nanocolumns [18]. As can be seen in the cross-sectional TEM image shown in **Figure 3a**, nanocolumns that are elongated along the whole GeMn layer are observed. A high-resolution TEM image shown in **Figure 3b** indicates that nanocolumns are coherent with the surrounding matrix and they have an average size of about 3–5 nm. By using electron energy-loss spectroscopy (EELS), the authors determined an average Mn concentration in nanocolumns ranging from 32 to 37.5% and attributed to a Ge_2Mn alloy, which does not exist in the Ge-Mn phase diagram.

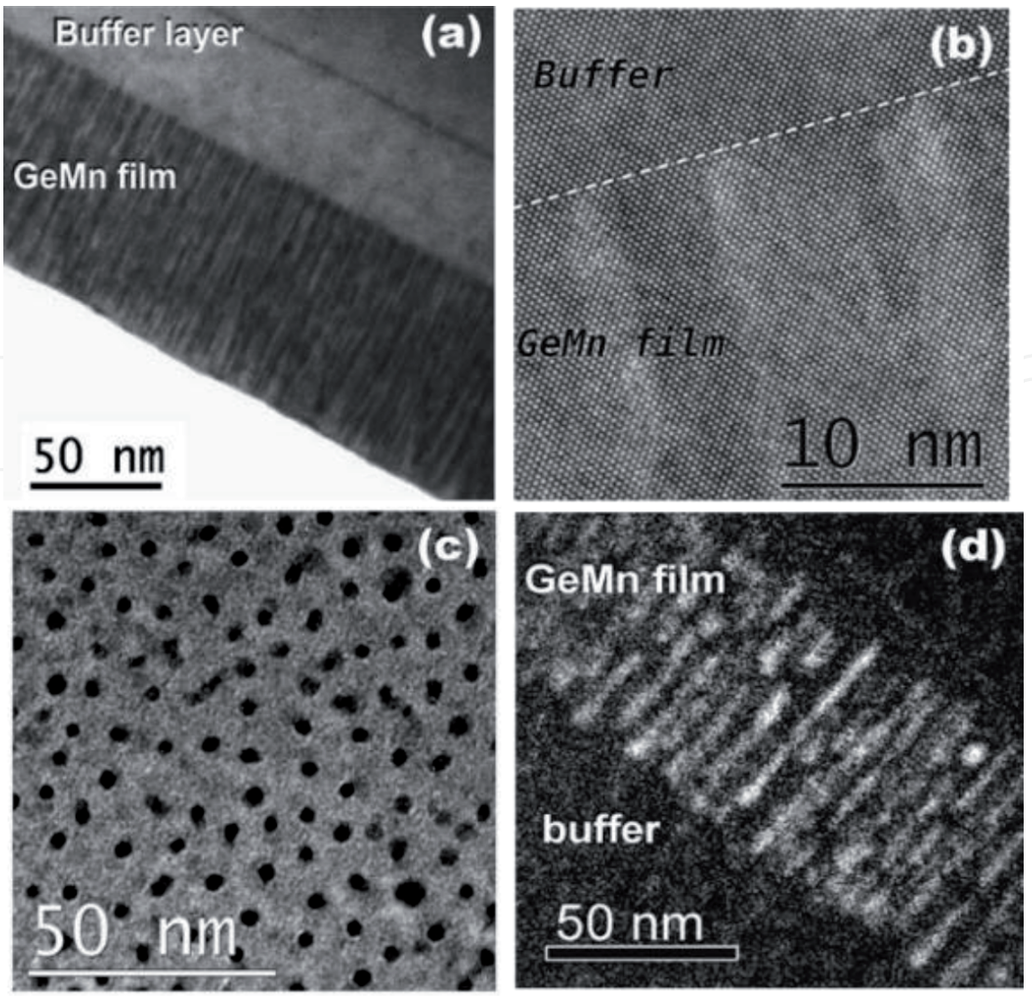

Figure 3.
Transmission electron micrographs of a Ge1–xMn$_x$ film grown at 130°C and containing 6% of manganese. (a) Cross section along the [110] axis; (b) High-resolution image of the interface between the Ge$_{1-x}$Mn$_x$ film and the Ge buffer layer; (c) Plane view micrograph performed on the same sample; (d) Mn chemical map obtained by energy-filtered transmission electron microscopy. Bright areas correspond to Mn-rich regions [39].

One of the most interesting features of this nanocolumn phase is that it exhibits magnetic ordering well above 400 K. The temperature dependence of magnetization of the corresponding sample is shown in **Figure 3a** of Ref. [25]. Magnetization of the layer persists at a temperature of 400 K, the upper limit of the instrument for magnetic measurements. Shown in the insert is the M(T) measurement after subtracting the magnetic signal of nanocolumns, much lower magnetic ordering is observed and has been attributed to a Mn-poor matrix between nanocolumns. It is worth noting that the above nanocolumns were shown to be stable up to 400°C and transformed into Mn_5Ge_3 clusters after 15 min of annealing at 650°C. This feature represents as a starting point of our research; our purpose consists of seeking the ways to stabilize this high-T_C nanocolumn phase.

3. Experiment detail

The solubility limit of Mn in Ge is very low (estimated to be 10^{15} cm^{-3} [37], corresponding to a Mn atomic concentration of ≈ 2×10^{-6} %). While using nonequilibrium growth techniques such as low-temperature MBE growth, a much higher Mn solubility has been demonstrated. However, such a low thermodynamical Mn solubility constitutes as the main obstacle to get homogeneous highly doped GeMn

films. On the other hand, the Mn dilution in a germanium crystal remains highly questionable and in most of experiments reported up to now; GeMn films are in general found to contain either nanoscaled Mn-rich regions or secondary-phase precipitates like Mn_5Ge_3. This means that it is crucial to combine nanoscale characterizations of the structural properties with magnetic properties in order get an accurate physical picture of grown films. The ultimate goal of research in GeMn materials could be thus find out growth techniques and growth conditions to obtain homogenous materials containing a few percent of Mn, allowing to raise the Curie temperature well above room temperature for the realization of spintronic devices. Up to now, low-temperature MBE technique has been intensively used to synthesize GeMn DMSs and promising results have been obtained [32, 33, 44, 46–48].

In our works, GeMn film growth was performed using solid source molecular beam epitaxy (MBE) on epi-ready Ge(001) wafers with a base pressure better than 1×10^{-10} Torr. Ge and Mn were evaporated using standard Knudsen effusion cells. The deposition chamber is equipped with RHEED to control the sample surface and to monitor the epitaxial growth process. The Ge deposition rate was estimated from RHEED intensity oscillations of the Ge-on-Ge homoepitaxy, whereas the Mn concentrations were deduced from Rutherford backscattering spectrometry (RBS) measurements. The cleaning of the Ge surfaces was carried out in two steps: the first was a chemical cleaning to eliminate hydrocarbon contaminants. Then, the Ge native oxide layers were etched in a diluted hydrofluoric acid solution (10%) for some minutes until a hydrophobic surface was obtained. The second step was an *in situ* thermal desorption of the surface oxide, which consists of outgassing the sample for several hours at 450°C followed by flash annealing at 750°C. After this step, a 40-nm-thick Ge buffer layer was grown at 250°C to ensure a good starting surface. Regarding the previous results, 80-nm-thick $Ge_{1-x}Mn_x$ films were subsequently grown at the substrate temperature of 130°C and Mn concentrations of ~6% to ensure the reproduction of GeMn nanocolumns.

Structural analyses of the grown films were performed through extensive high-resolution transmission electron microscopy (HR-TEM) by using a JEOL 3010 microscope operating at 300 kV with a spatial resolution of 1.7 Å. Imaging at this resolution requires TEM samples to be very thin in the region of interest. As a minimum requirement, samples must be electron transparent. To take advantage of a TEM's high resolution, it is necessary to prepare high-quality electron transparent samples. In practice, TEM specimens should be no thicker than 100 nm for low-resolution imaging and even thinner (~50 nm) for high-resolution imaging [49]. Sample preparation was carried out by standard mechanical polishing and argon ion milling. At first, the samples were cut in in two rectangular pieces (about 2 × 3 mm) and the film sides glued together with epoxy. Then, the samples were polished to a thickness of approximately 20 μm with a series of progressively smoother diamond papers. Gatan PIPS™ (Precision Ion Polishing System) ion mill was used for final thinning to electron transparency.

4. The surface signal of GeMn nanocolumn formation

The surface signal of nanocolumn phase is extremely important because this allows us to know if the nucleation of the nanocolumn phase takes place. **Figure 4** displays the evolution of RHEED patterns taken along the [1-10] azimuth of Ge surface during the growth of $Ge_{0.94}Mn_{0.06}$ film. Starting from RHEED pattern of the Ge surface prior to growth in **Figure 4a**, the Ge surface is characterized by a well-developed Ge reconstruction (2 × 1) streaky pattern, indicating that the surface is clean and smooth. This is also confirmed by the observation of high-intensity

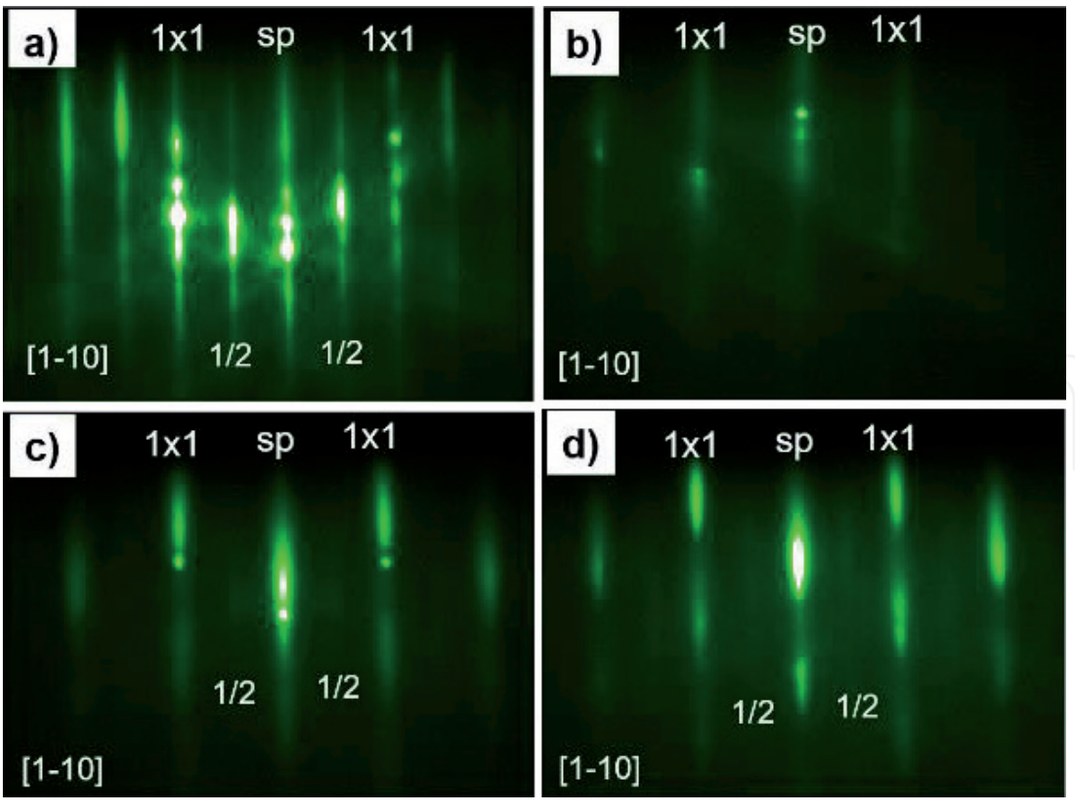

Figure 4.
RHEED patterns taken along the [1-10] azimuth of the clean Ge surface prior to growth (a), during the growth of the first monolayers (b), after 3 minutes of the growth (c), and finishing the growth process of ~80 nm $Ge_{1-x}Mn_x$ film (d), with Mn concentration ~ 6%.

Kikuchi lines, which overlap 1 × 1 and specular streaks, giving rise to localized reinforcements of intensity. The calculations of density functional theory (DFT) are in good agreement with these results and demonstrate that in the case of the clean surface Ge (001), the total energies are minimal for this type of symmetry [50]. The Ge reconstruction streak (2 × 1) disappears after a few monolayers of GeMn co-deposition (**Figure 4b**), then reappears in **Figure 4c**. The high-intensity spots due to the diffraction in transmission begin to appear on the 1 × 1 streaks after the deposition of a few nanometers and remain present until the end of the deposition (**Figure 4c** and **d**). This indicates the formation of a new GeMn phase having the same crystal structure as that of the Ge substrate. In addition, the surface of this new phase is rough. These three-dimensional (3D) spots come from the contribution of the nanocolumns that are formed in a diluted GeMn matrix whose structure is similar to that of Ge. Indeed, during homoepitaxy of Ge on Ge at this same growth temperature, the RHEED pattern presents diffraction streaks characteristic of two-dimensional growth. The observation this type of pattern is very interesting because it indicates that the growth surface is rough and that the degree of roughness remains constant during the deposition. In other words, the vertical growth speed of the area between the nanocolumns and that of the nanocolumns themselves are almost the same because the diffraction diagram remains unchanged. In addition, by comparing with the TEM images obtained, it is pointed out that the diameter of nanocolumns is smaller than the coherence length of the incident electron beam (10 nm), which makes it possible to attribute unambiguously the 3D spots on the 1 × 1 streaks of surface diffraction to the presence of the nanocolumn phase.

In short, in case of nanocolumn formation, the surface still exhibits a two-dimensional growth behavior although some intensity reinforcements at the Bragg diffraction positions are visible and the intensity of reconstructed ½ streaks

becomes weaker—the sign of GeMn nanocolumn formation of [51]. The 3D spots situated on the 1 × 1 streaks are the contribution of Mn-rich nanocolumns formed in the diluted GeMn matrix.

5. The growth direction and size of the GeMn nanocolumns

Figure 5 displays typical cross-sectional TEM images of a sample grown at 130°C and with Mn content of ~6%. Dark contrast corresponds to Mn-rich regions while regions with a brighter contrast arise from the diluted matrix. The corresponding film thickness is ~80 nm. According to an overall view of the layer structure, shown in low-scaled images in **Figure 5(a)**, we can see that the GeMn nanocolumns observed are very similar to those reported in Ref. 19. The self-assembled nanocolumns extend through the whole thickness of the GeMn layer. Most of nanocolumns are oriented perpendicular to the interface, that is, along the [001] direction. High-resolution TEM image taken around the nanocolumn inside the layer in **Figure 5(b)** reveals that nanocolumns are epitaxial and perfectly coherent with the surrounding diluted lattice. No defects nor presence of MnGe clusters are visible. **Figure 5(c)** shows that the interface is almost invisible and GeMn film exhibits the same diamond structure as Ge buffer layer. According to our previous study, at the growth temperature of Mn concentration of 6%, the nanocolumn can reach the maximum length of 80 nm before transforming into Mn_5Ge_3 clusters [52–54].

To investigate the arrangement and the size of GeMn nanocolumns, **Figure 6** displays the overall and high-resolution plan-view TEM images of 80-nm-thick $Ge_{0.94}Mn_{0.06}$ film. The nanocolumns are distributed evenly on the entire film surface with the diameter of about 5–8 nm. The inter-distance between adjacent columns is about 8–10 nm. The circle shape of Mn-rich nanocolumns in plan-view TEM images means that the GeMn nanocolumns exhibit cylindrical shape. Around each column in **Figure 6b**, a dark ring reveals a large strain extending over a few interatomic distances. The presence of a disordered core in the columns can reveal a plastic relaxation of the misfit stress with the surrounding matrix, probably due to the high-energy electron beam of the microscope. Studying the influence of Mn content

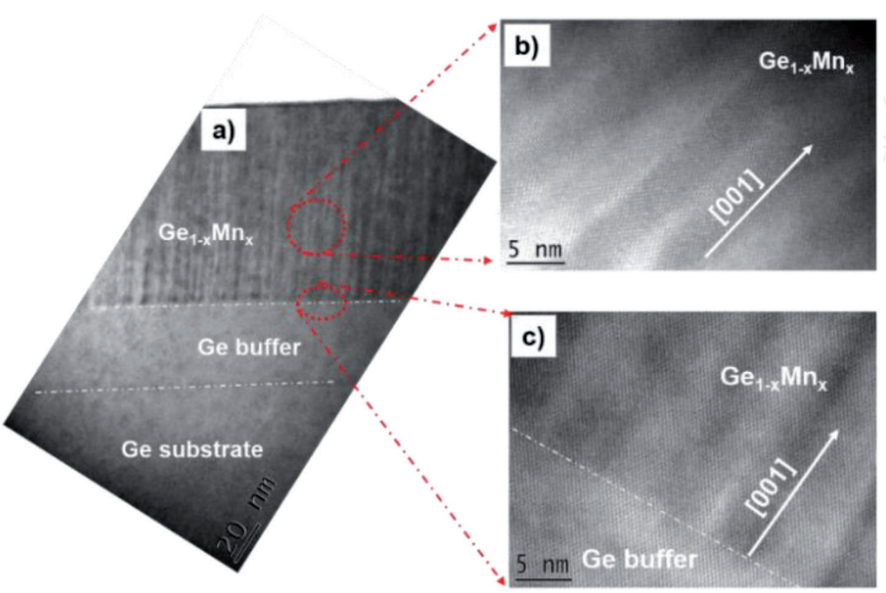

Figure 5.
Typical cross-sectional TEM image of a 80-n-thick $Ge_{1-x}Mn_x$ film with x ~ 0.06 (a), high-resolution TEM image taken inside the film (b) and around the interface region (c).

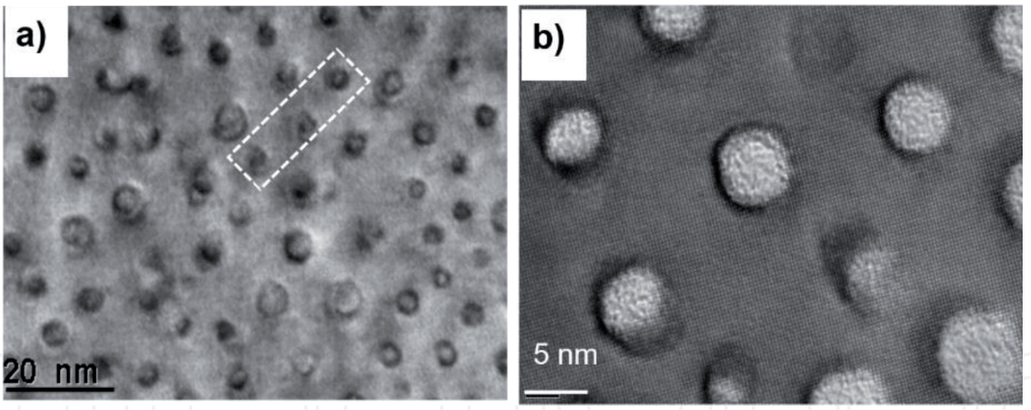

Figure 6.
Typical (a) and high-resolution (b) plan-view TEM image of a 80-nm-thick $Ge_{1-x}Mn_x$ film with x ~ 0.06.

on the formation of GeMn nanocolumns, previous studies show that increasing the Mn content leads to the column density remaining nearly constant, whereas their width increases and their height decreases drastically [39, 53].

In summary, GeMn nanocolumns are found to be formed at the Mn concentration of ~6%. We are thus able to stabilize the nanocolumn phase, which extends through the whole 80-nm thickness of the GeMn layer and exhibits the diamond structure elongated along the growth direction, with the diameter of about 5–8 nm.

6. Driving force for self-assembly and growth mechanisms of GeMn nanocolumns

The incorporation of impurities in a crystal lattice generally induces a constraint either at the local scale or in the whole lattice. With a very small amount of Mn (~6%), large-scale deformation is not expected. Since the atomic radius of an Mn atom (140 pm) is larger than that of a Ge atom (125 pm), the Mn-rich region, such as nanocolumns, should be in compression because of the presence of the Ge matrix surrounding them. The RHEED technique is very local but is not sufficient to be able to observe an infinitesimal constraint induced by nanocolumns. A Fourier transform of the cross-section TEM image inside the GeMn nanocolumn layers displayed in **Figure 7** shows that no dislocation can be observed in the filtered image along the Bragg's spots (220) of the red square area. This result indicates that the nanocolumn is in a stressed state. Note that filtering by the Fourier transform of the entire nanocolumn does not reveal any dislocation. It means that the nanocolumns are coherently strained in compression by the matrix along the growth direction. In any case, the presence of stress is inevitable even if the quantity of Mn incorporated is extremely small. The stress can be the important effect in the distribution of Mn atoms in the Ge matrix. A detailed study of the constraints would make it possible to better understand the mechanism of incorporation of Mn into nanocolumns and therefore to better understand the formation and growth kinetics of nanocolumns.

One of the central results concerning the nanocolumn formation is that the Mn concentration inside nanocolumns is not constant but increases from the interface to the film surface [55]. To understand the variation of the Mn concentration inside the $Ge_{1-x}Mn_x$ nanocolumns, we attempt to provide a phenomenological explanation of the $Ge_{1-x}Mn_x$ nanocolumn formation.

To investigate the mechanism leading to the formation of $Ge_{1-x}Mn_x$ nanocolumn, we recall that under nonequilibrium growth carried out at a temperature as low as 130°C, the Ge lattice can dilute a Mn concentration of about 0.25–0.5% [56].

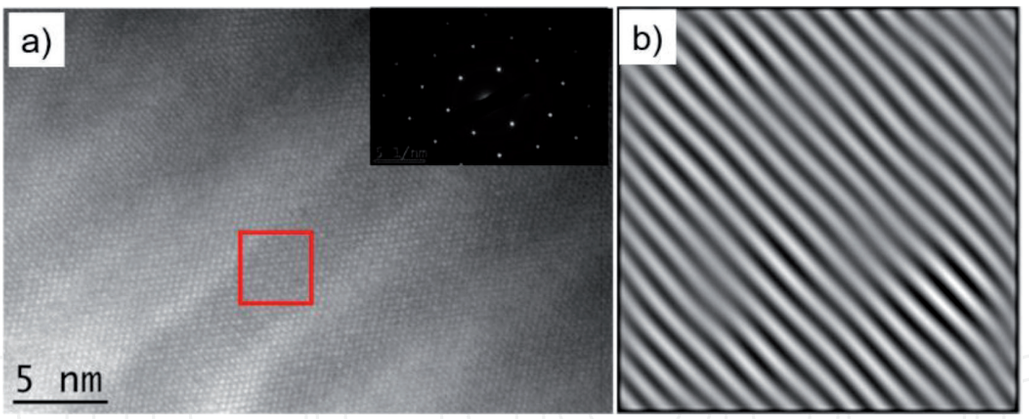

Figure 7.
High-resolution cross-section TEM image of the nanocolumns (a) and the image filtered along the Bragg's peak (220) of the red square area (b).

At the first stage of the growth, GeMn alloys with Mn concentration as high as ~6% are deposited on a Ge surface. This content far exceeds the solubility threshold of Mn atom in the Ge lattice. The excess Mn should diffuse and/or segregate along the surface to form Mn-rich regions. In other words, Mn-rich regions start to nucleate on the Ge surface even after deposition of the first monolayers and this is a direct consequence of the low solubility of Mn in the Ge lattice. The formation of these Mn-rich regions on the surface should "disturb" the surface morphology. This is what we have observed from RHEED patterns in **Figure 4b**. Probably, the presence of Mn-rich nuclei is responsible for the change in RHEED pattern of **Figure 4a** to RHEED pattern of **Figure 4b**. Since a too high Mn concentration in a nucleus is not favorable, both from the thermodynamical and epitaxial points of view, the system should self-organize to form nuclei with a certain density. The size of nuclei and the distance between nuclei depend on the Mn diffusion length on the film surface and the substrate temperature. Schema in **Figure 8** illustrates the formation of these Mn-rich nuclei on the Ge surface. During the GeMn deposition process, these nuclei may serve as seeds for the nanocolumn formation. **Figure 8** displays a schema illustrating the Mn accumulation on the Ge(001) surface.

The increase in Mn concentration within nanocolumns could be explained by vertical segregation of Mn along the [001] direction. The energy calculations along the Ge(001) orientation using spin-polarized density functional theory (DFT) show that

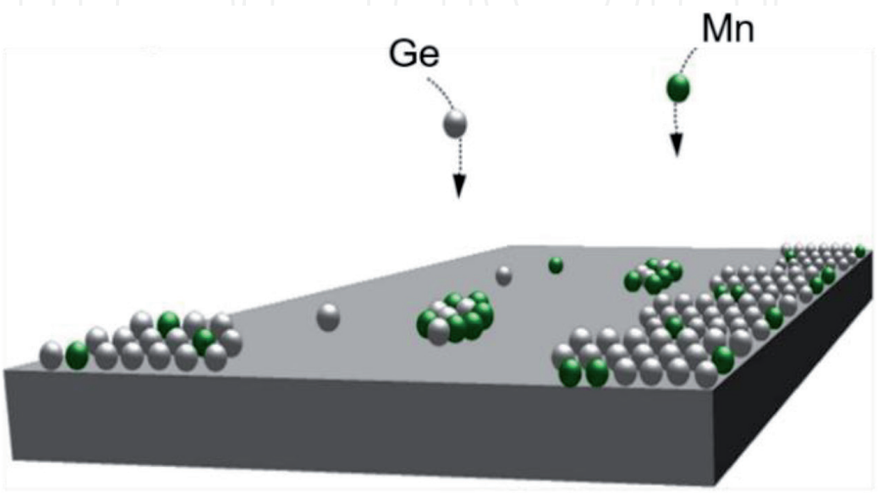

Figure 8.
The scheme of Mn accumulation on Ge(001) surface.

for Ge(100) −2 × 1 surface reconstruction, Mn diffuses via the surface interstitial site (I_0 site) preferentially. Mn adatoms originating from the gas phase or from deeper layers can easily diffuse toward the interstitial sites right beneath the dimers of Ge(100) −2 × 1 surface reconstruction. Therefore, growth of Mn-doped Ge(100) DMS at low temperatures should result in a high density of interstitial Mn. As Mn atoms are buried beneath a newly deposited Ge layer, they tend to float upward via the I_0 sites [44, 57]. Due to this surfactant effect of Mn atoms along the [001] direction, once Mn-rich nuclei are formed on the surface, further deposition leads to the formation of GeMn columns in which the Mn concentration continuously increases from interface to the film surface. And the cylindrical shape of nanocolumns allows them to minimize their interface energy with the surrounding diluted matrix. **Figure 9** displays a schema illustrating the segregation of Mn atoms during the growth GeMn nanocolumns.

According to our previous studies, the formation of GeMn nanocolumns and Mn_5Ge_3 clusters is a competing process [52]. During the growth, Mn continuously segregates toward the film surface and GeMn nanocolumns are found to transform to metallic Mn_5Ge_3 precipitates once the Mn concentration inside nanocolumns exceeds a highest value about 40%. It means that depending on the Mn concentration in the top of nanocolumns, nanocolumn growth can be interrupted. In the same time, other nanocolumns can start to nucleate in the middle of the layer if these regions are rich

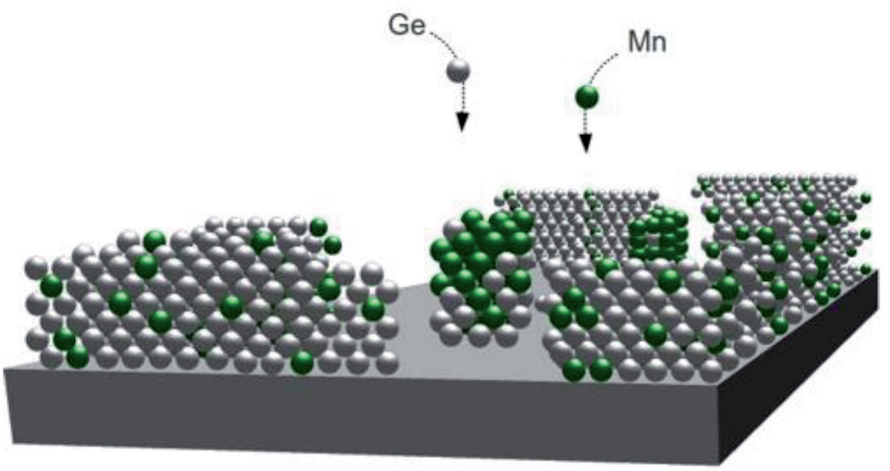

Figure 9.
The scheme of Mn atoms segregating toward the film surface through the interstitial sites during the deposition of $Ge_{1-x}Mn_x$ film on Ge(001) substrate.

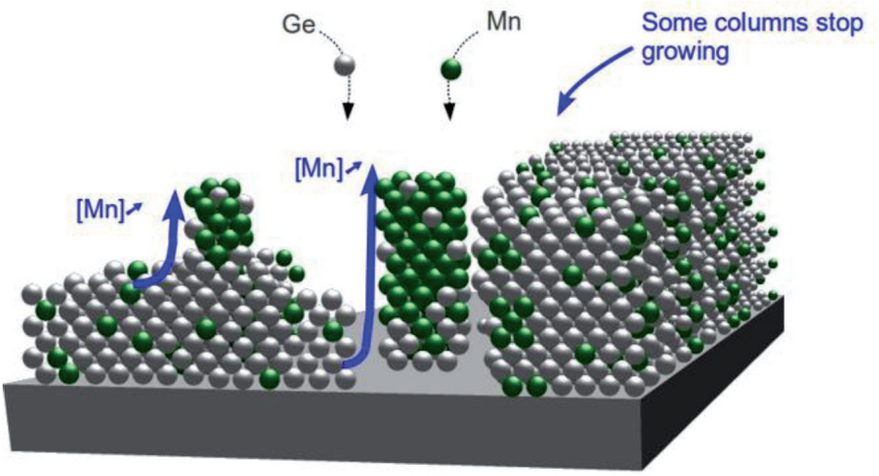

Figure 10.
The scheme of growth competition between $Ge_{1-x}Mn_x$ nanocolumns and Mn_5Ge_3.

enough in Mn to form new nuclei. **Figure 10** displays a schema illustrating the growth competition between $Ge_{1-x}Mn_x$ nanocolumns and Mn_5Ge_3 clusters.

Another interesting feature of nanocolumns is their core-shell structure [52, 53]. The Mn concentration across a nanocolumn is not homogenous; nanocolumns exhibit a core-shell structure with a much higher Mn concentration in the core compared to that of the shell. The Mn concentration in GeMn nanocolumns is highly inhomogeneous, it increases from interface to the film surface and also from the shell to the core of nanocolumns. Since the atomic radius of Mn atoms is slightly larger than that of Ge (127 and 122 picometers for Mn and Ge atoms, respectively), if the Mn concentration inside nanocolumns is too high, nanocolumns may exert a tensile strain on the surrounding lattice. To reduce such a strain, a core-shell structure with a reduced Mn concentration from core to shell should allow nanocolumns to more easily adapt the lattice parameter of the surrounding lattice. Thanks to this self-organized core-shell structure, almost all nanocolumns are found to be perfectly coherent with the surrounding lattice, as can be seen in **Figure 5**.

7. Conclusion

In conclusion, GeMn nanocolumns elongated along the growth direction are found to be formed at the growth temperature of 130°C and Mn concentration of ~6%. Based on the surface signals of GeMn nanocolumn formation, we are thus able to stabilize the nanocolumn phase, which exhibits the same diamond structure as Ge substrate with the diameter of about 5–8 nm and the maximum height of 80 nm. We have attempted to explain the nanocolumn formation using a phenomenological model based on Mn segregation and diffusion both in-plane and along the growth direction: (i) Mn-rich regions start to nucleate on the Ge surface even after deposition of the first monolayers and this is a direct consequence of the low solubility of Mn in the Ge lattice; (ii) due to the surfactant effect of Mn atoms along the [001] direction, further deposition leads to the formation of GeMn nanocolumns in which the Mn concentration continuously increases from interface to the film surface; (iii) GeMn nanocolumns become unstable when the Mn concentration reaches a value of 40% and then transform into Mn_5Ge_3 clusters. The shell-core structure of the column is formed to reduce strain, which is induced due to the difference in atomic radius between Ge and Mn.

Acknowledgements

The author thanks colleagues at Interdisciplinary Center of Nanoscience of Marseille (CINaM-CNRS), Aix-Marseille University, France for their technical help and fruitful discussions.

Author details

Thi Giang Le
Hong Duc University, Thanh Hoa, Vietnam

*Address all correspondence to: giangle74@gmail.com

References

[1] Wang R, Jiang X, Shelby RM, Macfarlane RM, Parkin SSP, Bank SR, et al. Label-free detection and classification of DNA by surface vibration spectroscopy in conjugation with electrophoresis. Applied Physics Letters. 2005;**86**:052901. DOI: 10.1063/1.1853529

[2] Jiang X, Wang R, Shelby RM, Macfarlane RM, Bank SR, Harris JS, et al. Highly spin-polarized room-temperature tunnel injector for semiconductor spintronics using MgO(100). Physical Review Letters. 2005;**94**:056601. DOI: 10.1103/PhysRevLett.94.056601

[3] van't Erve OMJ, Kioseoglou G, Hanbicki AT, Li CH, Jonker BT, Mallory R, et al. Comparison of Fe/Schottky and $Fe/Al_2O_3Fe/Al_2O_3$ tunnel barrier contacts for electrical spin injection into GaAs. Applied Physics Letters. 2004;**84**:4334. DOI: 10.1063/1.1758305

[4] Li CH, Kioseoglou G, van't Erve OMJ, Hanbicki AT, Jonker BT, Mallory R, et al. Spin injection across (110) interfaces: Fe/GaAs(110)Fe/GaAs(110) spin-light-emitting diodes. Applied Physics Letters. 2004;**85**:1544. DOI: 10.1063/1.1810534

[5] Olive Mendez S, Le Thanh V, Ranguis A, Derrien J. Growth of magnetic materials and structures on Si(0 0 1) substrates using Co_2Si as a template layer. Applied Surface Science. 2008;**254**:6040. DOI: 10.1016/j.apsusc.2008.02.193

[6] Olive-Mendez SF, Spiesser A, Michez LA, Le Thanh V, Glachant A, Derrien J, et al. Epitaxial growth of Mn_5Ge_3/Ge(111) heterostructures for spin injection. Thin Solid Films. 2008;**517**:191. DOI: 10.1016/j.tsf.2008.08.090

[7] Matsukura F, Ohno H, Shen A, Sugawara Y. Transport properties and origin of ferromagnetism in (Ga,Mn)As. Physical Review B. 1998;**57**:R2037. DOI: 10.1103/PhysRevB.57.R2037

[8] Jungwirth T, Wang KY, Masek J, Edmonds KW, Konig J, Sinova J, et al. Prospects for high temperature ferromagnetism in (Ga,Mn) As semiconductors. Physical Review B. 2005;**72**:165204. DOI: 10.1103/PhysRevB.72.165204

[9] Zutic I, Fabian J, Erwin SC. Spin injection and detection in silicon. Physical Review Letters. 2006;**97**:026602. DOI: 10.1103/PhysRevLett.97.026602

[10] Zhang FM, Liu XC, Gao J, Wu XS, Du YW, Zhu H, et al. Investigation on the magnetic and electrical properties of crystalline $Mn_{0.05}Si_{0.95}$ films. Applied Physics Letters. 2004;**85**:786. DOI: 10.1063/1.1775886

[11] Zhou S, Potzger K, Zhang G, Mucklich A, Eichhorn F, Schell N, et al. Structural and magnetic properties of Mn-implanted Si. Physical Review B. 2007;**75**:085203. DOI: 10.1103/PhysRevB.75.085203

[12] Ko V, Teo KL, Liew T, Chong TC, MacKenzie M, MacLaren I, et al. Origins of ferromagnetism in transition-metal doped Si. Journal of Applied Physics. 2008;**104**:033912. DOI: 10.1103/PhysRevB.78.045307

[13] Yabuuchi S, Kageshima H, Ohno Y, Nagase M, Fujiwara A, Ohta E. Origin of ferromagnetism of MnSi1.7 nanoparticles in Si: First-principles calculations. Physical Review B. 2008;**78**:045307. DOI: 10.1103/PhysRevB.78.045307

[14] Zwicker U, Jehn E, Schubert E. A study of the manganese-germanium system. Zeitschrift fuer MetaIlkunde. 1949;**40**:433

[15] Predel B. Ge-Mn (Germanium-Manganese). Landolt-Börnstein—Group IV Physical Chemistry, Volumn 5F. SpringerMaterials. 1996. DOI: 10.1007/10501684_1481

[16] Park YD, Hanbicki AT, Erwin SC, Hellberg CS, Sullivan JM, Mattson JE, et al. A group-IV ferromagnetic semiconductor: Mn_xGe_{1-x}. Science. 2002;**295**:651. DOI: 10.1126/science.1066348

[17] Ahlers S, Bougeard D, Sircar N, Abstreiter G, Trampert A, Opel M, et al. Magnetic and structural properties of Ge_xMn_{1-x} films: Precipitation of intermetallic nanomagnets. Physical Review B. 2006;**74**:214411. DOI: 10.1103/PhysRevB.74.214411

[18] Devillers T. Ferromagnetic phases of Ge(1−x)Mn(x) for spintronics applications [PhD thesis]. Grenoble: Université Joseph Fourier; 2008

[19] Li H. Fabrication and characterization of nanostructured half metals and diluted magnetic semiconductors [PhD thesis] Singapore: National University of Singapore; 2006

[20] Fert A, Jaffrès H. Conditions for efficient spin injection from a ferromagnetic metal into a semiconductor. Physical Review B. 2001;**64**:184420. DOI: 10.1103/PhysRevB.64.184420

[21] Padova PD, Ayoub J-P, Berbezier I, Perfetti P, Quaresima C, Testa AM, et al. $Mn_{0.06}Ge_{0.94}$ diluted magnetic semiconductor epitaxially grown on Ge(001): Influence of Mn_5Ge_3 nanoscopic clusters on the electronic and magnetic properties. Physical Review B. 2008;**77**:045203. DOI: 10.1103/PhysRevB.77.045203

[22] Morresi L, Ayoub J, Pinto N, Ficcadenti M, Murri R, Ronda A, et al. Formation of Mn_5Ge_3 nanoclusters in highly diluted Mn_xGe_{1-x} alloys. Materials Science in Semiconductor Processing. 2006;**9**:836. DOI: 10.1016/j.mssp.2006.08.056

[23] Bihler C, Jaeger C, Vallaitis T, Gjukic M, Brandt MS, Pippel E, et al. Structural and magnetic properties of Mn_5Ge_3 clusters in a dilute magnetic germanium matrix. Applied Physics Letters. 2006;**88**:112506. DOI: 10.1063/1.2185448

[24] Park YD, Wilson A, Hanbicki AT, Mattson JE, Ambrose T, Spanos G, et al. Magnetoresistance of Mn:Ge ferromagnetic nanoclusters in a diluted magnetic semiconductor matrix. Applied Physics Letters. 2001;**78**:2739. DOI: 10.1063/1.1369151

[25] Jamet M, Barski A, Devillers T, Poydenot V, Dujardin R, Bayle-Guillemaud P, et al. High-curie-temperature ferromagnetism in self-organized $Ge_{1-x}Mn_x$ nanocolumns. Nature Materials. 2006;**5**:653. DOI: 10.1038/nmat1686

[26] Olive Mendez SF, Petit M, Ranguis A, Le Thanh V, Michez L-A. From the very first stages of Mn deposition on Ge(001) to phase segregation. Crystal Growth & Design. 2018;**18**:5124-5129. DOI: 10.1021/acs.cgd.8b00558

[27] Alvídrez-Lechuga A, Holguín JT, Solís-Canto Ó, Santillán-Rodríguez CR, Matutes-Aquino JA, Olive-Méndez SF. Surface-interface quality of Mn_5Ge_3 thin films on Ge(001): Reactive deposition epitaxy vs. solid phase epitaxy. Microscopy and Microanalysis. 2018;**24**:1622. DOI: 10.1017/S1431927618008590

[28] Schütz MK, Petit M, Michez L, Ranguis A, Monier G, Robert Goumet C, et al. Thiol-functionalization of Mn_5Ge_3 thin films. Applied Surface Science. 2018;**451**:191-197. DOI: 10.1016/j.apsusc.2018.04.231

[29] Pinto N, Morresi L, Ficcadenti M, Murri R, D'Orazio F, Lucari F, et al. Magnetic and electronic transport percolation in epitaxial $Ge_{1-x}Mn_x$ films. Physical Review B. 2005;**72**:165203. DOI: 10.1103/PhysRevB.72.165203

[30] Tsui F, He L, Ma L, Tkachuk A, Chu YS, Nakajima K, et al. Novel germanium-based magnetic semiconductors. Physical Review Letters. 2003;**91**:177203. DOI: 10.1103/PhysRevLett.91.177203

[31] Michez L, Spiesser A, Petit M, Bertaina S, Jacquot JF. Magnetic reversal in Mn_5Ge_3 thin films: An extensive study. Journal of Physics: Condensed Matter. 2015;**27**(26):266001. DOI: 10.1088/0953-8984/27/26/266001

[32] Li AP, Wendelken JF, Shen J, Feldman LC, Thompson JR, Weitering HH. Magnetism in Ge_{1-x} Mn_x semiconductors mediated by impurity band carriers. Physical Review B. 2005;**72**:195205

[33] Xie Y, Yuan Y, Mao W, Xu C, Hübner R, Grenzer J, et al. Epitaxial Mn_5Ge_3 (100) layer on Ge(100) substrates obtained by flash lamp annealing. Applied Physics Letters. 2018;**113**:222401. DOI: 10.1063/1.5057733

[34] Petit M, Boussadi A, Heresanu V, Ranguis A, Michez L. Step flow growth of Mn_5Ge_3 films on Ge(111) at room temperature. Applied Surface Science. 2019;**480**:529-536. DOI: 10.1016/j.apsusc.2019.01.164

[35] Kang JS, Kim G, Wi SC, Lee SS, Choi S, Cho S, et al. Spatial chemical inhomogeneity and local electronic structure of Mn-doped Ge ferromagnetic semiconductors. Physical Review Letters. 2005;**94**:147202. DOI: 10.1103/PhysRevLett.94.147202

[36] Picozzi S, Ottaviano L, Passacantando M, Profeta G, Continenza A, Priolo F, et al. X-ray absorption spectroscopy in Mn_xGe_{1-x} diluted magnetic semiconductor: Experiment and theory. Applied Physics Letters. 2005;**86**:062501. DOI: 10.1063/1.1861127

[37] Woodbury HH, Tyler WW. Properties of germanium doped with manganese. Physics Review. 1995;**100**:659. DOI: 10.1103/PhysRev.100.659

[38] Li AP, Zeng C, van Benthem K, Chisholm MF, Shen J, Rao SVSN, et al. Dopant segregation and giant magnetoresistance in manganese-doped germanium. Physical Review B. 2007;**75**:201201. DOI: 10.1103/PhysRevB.75.201201

[39] Devillers T, Jamet M, Barski A, Poydenot V, Bayle-Guillemaud P, Bellet-Amalric E, et al. Structure and magnetism of self-organized $Ge_{1-x}Mn_x$ nanocolumns on Ge(001). Physical Review B. 2007;**76**:205306. DOI: 10.1103/PhysRevB.76.205306

[40] Gambardella P, Claude L, Rusponi S, Franke KJ, Brune H, Raabe J, et al. Surface characterization of Mn_xGe_{1-x} and $Cr_yMn_xGe_{1-x-y}$ dilute magnetic semiconductors. Physical Review B. 2007;**75**:125211. DOI: 10.1103/PhysRevB.75.125211

[41] Biegger E, Staheli L, Fonin M, Rudiger U, Dedkov YS. Intrinsic ferromagnetism versus phase segregation in Mn-doped Ge. Journal of Applied Physics. 2007;**101**:103912. DOI: 10.1063/1.2718276

[42] Bougeard D, Ahlers S, Trampert A, Sircar N, Abstreiter G. Clustering in a precipitate-free GeMn magnetic semiconductor. Physical Review Letters. 2006;**97**:237202. DOI: 10.1103/PhysRevLett.97.237202

[43] Bougeard D, Sircar N, Ahlers S, Lang V, Abstreiter G, Trampert A, et al. Ge_{1-x} Mn_x clusters: Central structural

and magnetic building blocks of nanoscale wire-like self-assembly in a magnetic semiconductor. Nano Letters. 2009;**9**:3743. DOI: 10.1021/nl901928f

[44] Zeng C, Zhang Z, van Benthem K, Chisholm MF, Weitering HH. Optimal doping control of magnetic semiconductors via subsurfactant epitaxy. Physical Review Letters. 2008;**100**:066101. DOI: 10.1103/PhysRevLett.100.066101

[45] Ahlers S, Stone PR, Sircar N, Arenholz E, Dubon OD, Bougeard D. Comparison of the magnetic properties of GeMn thin films through Mn L-edge x-ray absorption. Applied Physics Letters. 2009;**95**:151911. DOI: 10.1063/1.3232245

[46] Ahlers S, Bougeard D, Riedl H, Abstreiter G, Trampert A, Kipferl W, et al. Ferromagnetic Ge(Mn) nanostructures. Physica E: Low-dimensional Systems and Nanostructures. 2006;**32**:422. DOI: 10.1016/j.physe.2005.12.129

[47] Ahlers S. Magnetic and structural properties of Ge_{1-x} Mn_x films: Precipitation of intermetallic nanomagnets. Physical Review B. 2006;**74**:214411. DOI: 10.1103/PhysRevB.74.2144

[48] Holy V. Diffuse x-ray scattering from inclusions in ferromagnetic Ge_{1-x} Mn_x layers. Physical Review B. 2008;**78**:144401. DOI: 10.1103/PhysRevB.78.144401

[49] Sarney WL. Sample Preparation Procedure for TEM Imaging of Semiconductor Materials. Adelphi, Maryland: U.S. Army Research Laboratory; 2004. ARL-TR-3223; Corpus ID: 139408847

[50] Needels M, Payne MC, Joannopoulos JD. High-order reconstructions of the Ge(100) surface. Physical Review B. 1998;**38**(8):5543-5546. DOI: 10.1103/physrevb.38.5543

[51] Le TG. Direct structural evidences of epitaxial growth $Ge_{1-x}Mn_x$ nanocolumn bi-layers on Ge(001). Materials Sciences and Applications. 2015;**6**:533-538. DOI: 10.4236/msa.2015.66057

[52] Le TG, Dau M-T, Le Thanh V, Nam DNH, Petit M, Michez LA, et al. Growth competition between semiconducting $Ge_{1-x}Mn_x$ nanocolumns and metallic Mn_5Ge_3 clusters. Advances in Natural Sciences: Nanoscience and Nanotechnology. 2012;**3**:025007. DOI: 10.1088/2043-6262/3/2/025007

[53] Le TG, Nam DNH, Dau M-T, TKP L, Khiem NV, Le Thanh V, et al. The effects of Mn concentration on structural and magnetic properties of $Ge_{1-x}Mn_x$ diluted magnetic semiconductor. Journal of Physics: Conference Series. 2011;**292**:012012. DOI: 10.1088/1742-6596/292/1/012012

[54] Le TG, Le Thanh V, Michez L. Effect of carbon on structural and magnetic properties of $Ge_{1-x}Mn_xGe_{1-x}Mn_x$ nanocolumns. Bulletin of Materials Science. 2020;**43**:103. DOI: 10.1007/s12034-020-2082-z

[55] Le TG, Nuyen MA. Chemical composition of high-T_C $Ge_{1-x}Mn_x$ nanocolumns grown on Ge(001) substrates. Communications in Physics. 2014;**24**(2):163-169

[56] Le TG, Dau MT. Vertical self-organization of $Ge_{1-x}Mn_x$ nanocolumn multilayers grown on Ge(001) substrates. Modern Physics Letters B. 2016;**30**:1650269. DOI: 10.1142/S0217984916502699

[57] Zhu W, Weitering HH, Wang EG, Kaxiras E, Zhang Z. Contrasting growth modes of Mn on Ge(100) and Ge(111) surfaces: Subsurface segregation versus intermixing. Physical Review Letters. 2004;**93**:126102. DOI: 10.1103/PhysRevLett.93.126102